Engineered nanoparticles for systemic siRNA delivery to malignant brain tumours†

Johan Karlsson,[a,b,c] Yuan Rui,[a,b] Kristen L. Kozielski,[a,b] Amanda L. Placone,[b,c]
Olivia Choi,[a,b] Stephany Y. Tzeng,[a,b] Jayoung Kim,[a,b] Jamal J. Keyes,[a,b]
Max I. Bogorad,[b,c] Kathleen Gabrielson,[d] Hugo Guerrero-Cazares,[e]
Alfredo Quiñones-Hinojosa,[e] Peter C. Searson (ID) *[b,c] and
Jordan J. Green (ID) *[a,b,c,f,g,h]

Improved delivery materials are needed to enable siRNA transport across biological barriers, including the blood–brain barrier (BBB), to treat diseases like brain cancer. We engineered bioreducible nanoparticles for systemic siRNA delivery to patient-derived glioblastoma cells in an orthotopic mouse tumor model. We first utilized a newly developed biomimetic *in vitro* model to evaluate and optimize the performance of the engineered bioreducible nanoparticles at crossing the brain microvascular endothelium. We performed transmission electron microscopy imaging which indicated that the engineered nanoparticles are able to cross the BBB endothelium *via* a vesicular mechanism. The nanoparticle formulation engineered to best cross the BBB model *in vitro* led to safe delivery across the BBB to the brain *in vivo*. The nanoparticles were internalized by human brain cancer cells, released siRNA to the cytosol *via* environmentally-triggered degradation, and gene silencing was obtained both *in vitro* and *in vivo*. This study opens new frontiers for the *in vitro* evaluation and engineering of nanomedicines for delivery to the brain, and reports a systemically administered biodegradable nanocarrier for oligonucleotide delivery to treat glioma.

Introduction

Glioblastoma is one of the most lethal cancers and, despite optimal treatment, the median survival is only 12 to 15 months for patients diagnosed with glioblastoma, and

[a]Department of Biomedical Engineering and the Translational Tissue Engineering Center, Johns Hopkins University School of Medicine, Baltimore, MD 21231, USA. E-mail: green@jhu.edu
[b]Institute for Nanobiotechnology, Johns Hopkins University, Baltimore, MD 21218, USA. E-mail: searson@jhu.edu
[c]Department of Materials Science and Engineering, Johns Hopkins University, Baltimore, MD 21218, USA
[d]Department of Molecular and Comparative Pathobiology, Johns Hopkins University School of Medicine, Baltimore, MD 21231, USA
[e]Department of Neurosurgery, Mayo Clinic Florida, Jacksonville, FL 32224, USA
[f]Departments of Neurosurgery, Oncology, and Ophthalmology, Johns Hopkins University School of Medicine, Baltimore, MD 21231, USA
[g]Department of Chemical and Biomolecular Engineering, Johns Hopkins University, Baltimore, MD 21231, USA
[h]Sidney Kimmel Comprehensive Cancer Center and the Bloomberg~Kimmel Institute for Cancer Immunotherapy, Johns Hopkins University School of Medicine, Baltimore, MD 21231, USA
†Electronic supplementary information (ESI) available: Full experimental details, TEM image of the setup for the *in vitro* blood–brain barrier permeability assay (Fig. S1), LI-COR results of the nanoparticles biodistribution *in vivo* (Fig. S2), and toxicity studies (Fig. S3 and S4). See DOI: 10.1039/c9nr04795f

nearly all malignant gliomas eventually recur.[1–3] New improved chemotherapies have the potential to improve the clinical outcomes, however, most drug candidates do not traverse the blood–brain barrier (BBB) and hence cannot reach the tumours. The brain microvascular endothelial cells (BMECs) that form the lumen of the cerebrovasculature express tight junctions (TJs) which effectively block paracellular transport, and an array of multi-spectrum efflux pumps which recycle small molecules back into circulation.[4,5] As a result, less than 2% of potential small molecule drugs and almost no macromolecular drugs are able to enter the brain, and this has hampered the development of efficient therapeutic treatments of glioma.[6] The design of drug delivery systems that could encapsulate cargos and exploit innate transport processes to enter the brain are essential to enable new therapeutic treatments of glioma.

In recent years, new insights have provided understanding of molecular abnormalities underlying glioma pathogenesis and have highlighted the use of gene delivery to provide new glioma treatment paradigms.[1,7–9] Successful gene delivery has the potential to reprogram glioma cells to influence multiple pathways including cellular proliferation, cellular survival, invasion, and angiogenesis.[1] Small interfering RNA (siRNA) molecules have the ability to inhibit sequence-specific intracellular protein synthesis involved in the progression of glioma. To achieve therapeutic potency of siRNA, safe and

effective delivery methods are needed. Unmodified siRNA is rapidly enzymatic degraded in the blood stream, can be immunogenic, does not readily enter cells, and is unable to efficiently escape the endosomal compartment to reach the cytosol.[10–12] Therefore, delivery vehicles are required to achieve efficient intracellular delivery of oligonucleotides for unmet therapeutic needs.[13–16] A broad variety of materials have been employed to enable efficient siRNA delivery, such as lipid-based,[14,15,17] inorganic,[18–21] and polymeric materials.[22–25] Due to the challenge of crossing the BBB, the conventional approach for gene therapy has been to inject the vector used to transport the siRNA or DNA molecules locally to the brain.[26] However, local delivery is less clinically relevant due to the invasiveness of the surgery required to access the brain and the difficulty in reaching all of the cells in a tumour that is often diffuse. Hence, there is a need for drug delivery systems. For effective systemic siRNA delivery, the drug delivery system must resist serum nucleases, prevent renal clearance, facilitate exit from blood vessels to the targeted tissue, enable entry into targeted cells, and induce intracellular release.[10,12] Such a system would be enabling for the treatment of brain cancer as well as many other neurological diseases. The use of cationic polymers to encapsulate siRNA into nanoparticles (NPs) for delivery could potentially facilitate transport to the brain. Not only would the polymer's positive charge enable complexation to anionic siRNA, but these nanoparticles could potentially also facilitate transport across the BBB through adsorptive mediated transport (AMT),[27,28] using a mechanism that mimics the natural transport of polycationic proteins. The concept of AMT is based on observations of the polycationic protein protamine, which binds to the BBB endothelial cell surface and then induces cellular uptake and transport into the brain parenchyma.[29,30]

Biodegradable poly(β-amino ester)s (PBAE) have been reported as effective nanocarriers to provide effective DNA delivery,[31–36] and more recently with new polymer structural modifications, have shown promise for siRNA delivery in vitro.[37] We recently demonstrated that specific polymer modifications to PBAEs to incorporate disulfide bonds and make the nanomaterials bioreducible can enable preferential in vitro delivery of siRNA to patient-derived glioblastoma (GBM) cells over healthy neural progenitor cells via biomaterial-mediated intrinsic targeting.[38]

In this current work, we sought to develop nanoparticles that are stable in serum, bioreducible in an intracellular environment, and allow transport across the BBB to enable siRNA delivery to GBM cells via systemic administration. The intrinsic ability of a polymer to protect systemically administered siRNA from degradation and deliver it across the BBB is desirable to open up new biological therapies for brain cancer and other neurological disorders. To create nanomedicines capable of transport to the brain, we first utilized a newly reported cell line in a BBB in vitro assay to evaluate whether specific properties of nanoparticles could overcome the major hurdle of BBB crossing and enable systemically administered siRNA to reach glioblastoma cells. To assess transport across

the human BBB, we performed transport studies with human brain microvascular endothelial cells (hBMEC) derived from human induced pluripotent stem cells (iPSCs).[39,40] The leading nanomedicine from our in vitro studies was subsequently validated for delivery across the BBB to malignant brain tumours in vivo.

Experimental

Materials

The chemicals used in the synthesis of the base monomer BR6 were all purchased from Sigma-Aldrich (St Louis, MO, USA). The other monomers (S4, E6, and E7) used in the polymer syntheses were purchased from Alfa Aesar (Ward Hill, MA, USA). The siRNA targeting eGFP and negative control siRNA used as the scrambled RNA (scRNA) were purchased from Life Technologies (Carlsbad, CA, USA). AllStars Human Cell Death siRNA was purchased from Qiagen (Germantown, MD, USA), and the siRNA targeting luciferase from OriGene (Rockville, MD, USA).

Syntheses of base monomer BR6 and polymers

See ESI† for full details on the synthesis procedure. In brief, the base monomer 2,2′-disulfane-diylbis(ethane-2,1-diyl) (BR6) was synthesized by reacting a solution of bis(2-hydroxyethyl)disulfide (15.4 g, 10 mmol), triethylamine (TEA, 37.5 mL, 300 mmol), and THF with acryloyl chloride (300 mmol) following the methods of Kozielski et al.[38] The PBAEs were synthesized using a two-step reaction, in a similar manner to what Bhise et al. previously reported.[41] The diacrylate backbone monomer, BR6, was polymerized to the side chain monomer, 4-amino-1-butanol (S4), using Michael addition as synthesis method. As a second step, the diacrylate-terminated base polymer (BR6-S4) were end-capped using either 2-(3-(aminopropyl)-amino)methanol (E6) or 1-(3-aminopropyl)-4-methyl-piperazine (E7). The polymer synthesis for polymers R646 and R647 is shown in Fig. 1.
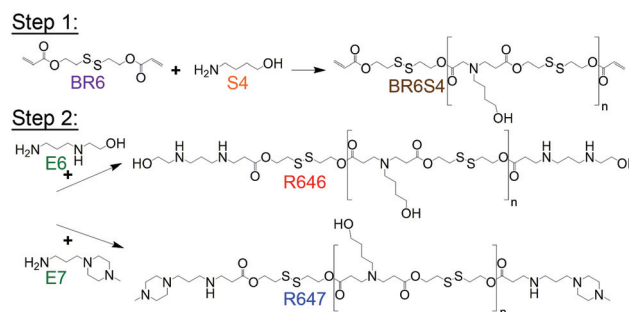
Fig. 1 Scheme of the two-step synthesis to form the polymers R646 and R647 used as the nanocarriers for siRNA delivery. In the first step, the diacrylate backbone monomer BR6 is polymerized with the side chain monomer S4, and the resulting base polymer BR6S4 was in the second step endcapped by either E6 or E7 to form R646 or R647, respectively.

Characterization of physical properties for the bioreducible PBAE-siRNA nanoparticles

Dynamic light scattering (DLS) measurements using a Malvern Zetasizer NanoZS (Malvern Instruments, Worcestershire, UK) was performed to determine the hydrodynamic diameter and surface charge of the prepared nanoparticles loaded with siRNA. We carried out DLS measurements both in PBS and in culture medium containing 10% fetal bovine serum (FBS; Invitrogen, Carlsbad, CA, USA). Furthermore, the nanoparticle size measurements in 10% FBS medium were carried out at specific timepoints until 4 h being the endpoint. The nanoparticles were formed by mixing the polymer and siRNA in 25 mM of sodium acetate (NaAc) (pH = 5.0) for 10 min to ensure complete self-assembly between the polymer and siRNA molecules. The analysed nanoparticle formulation was formed with a polymer (R646 or R647) concentration of 180 μg mL^{-1} and the different doses of siRNA were 10, 60, or 120 nM.

Transmission electron microscopy (TEM) was also employed to examine the nanoparticle size and shape. The prepared formulations had a polymer (R646 or R647) concentration of 180 μg mL^{-1} and a siRNA dose of 10 nM. The different nanoparticle formulations were diluted in PBS, thereafter added onto the carbon-coated copper TEM grids (Electron Microscopy Sciences, Hatfield, PA, USA) and allowed to dry prior to TEM analysis. The TEM characterization was carried out using a FEI Tecnai 12 TWIN TEM (FEI, Hillsboro, OR, USA) microscope, operated at 120 kV. The TEM images were acquired using a SIS Megaview III wide-angle CCD camera. The software ImageJ (National Institutes of Health, Bethesda, MD, USA) was used to measure the nanoparticle diameter in the acquired TEM micrographs.

In the gel electrophoresis assay, nanoparticles were formed at 1200 w/w, 200 w/w, and 100 w/w ratios between the polymer and siRNA which corresponds to the nanoparticles being loaded with 10, 60, or 120 nM siRNA, respectively. In the assay, the siRNA dose was kept constant at 0.0025 mg mL^{-1} for all the analysed formulations. The formed nanoparticles were incubated at 1 : 10 (v/v) ratio at 37 °C for 4 h in PBS or culture medium containing 10% serum to examine the encapsulation stability of the siRNA load, and up to 1 h in PBS containing 5 mM L-glutathione (GSH; Thermo Scientific, Rockford, IL, USA) to analyse the siRNA release in an environment mimicking the cytosol. At each timepoint, a 20 μL sample volume was collected and a solution of 30% glycerol was added to the different conditions in a 1 : 5 (v/v) ratio. The samples were subsequently added to an 1% agarose gel containing 1 μg mL^{-1} ethidium bromide and the electrophoresis proceed for 20 min at 100 mV. The gels were thereafter imaged using UV light exposure.

Nanoparticle tracking analysis (NTA) was performed using a Nanosight NS500 (Malvern, Westborough, MA, USA to determine the nanoparticle concentrations and siRNA loading per nanoparticle. For each measurement, the nanoparticles were diluted a 150-fold in PBS using a two-step dilution to obtain 20–100 particles per frame in the Nanosight software. Three independent samples were analysed from each group. The nanoparticle concentration measured through NTA was determined as particles per volume, and based on this value and that all doses of siRNA were found to be 100% encapsulated in the nanoparticles as observed by the gel electrophoresis assays (Fig. 3), the siRNA loading per nanoparticle could be calculated algebraically be dividing the known concentration of siRNA molecules by the measured concentration of nanoparticles.

In vitro blood–brain barrier permeability

The nanoparticle permeability was evaluated across monolayers of hBMECs seeded in transwells. hBMECs were derived from BC1 human induced pluripotent stem cells (iPSCs) based on a protocol reported by Lippman and coworkers.[39,42] hBMECs derived from human iPSCs were seeded in transwells (24 well; 0.33 cm^2 surface area; polyester membrane; 3.0 μm pore diameter; Corning) for permeability measurements. Prior to the experiments, the transwells were coated with a 50/50 mixture of 100 μg mL^{-1} collagen IV (BD Biosciences, San Jose, CA, USA) and 50 μg mL^{-1} fibronectin (BD Biosciences) overnight as described by Katt et al.[40] The hBMECs cells were thereafter seeded at a density of 1 × 10^6 cells per mL two days prior to permeability experiments. The medium was changed prior to the experiment to culture medium using DMEM/F-12 medium without phenol red (Invitrogen), 10% FBS (Invitrogen), and 1% penicillin–streptomycin (Life Technologies) to reduce the degree of autofluorescence from the media. Transendothelial electrical resistance (TEER) measurements were performed in each well using an EVOM^2 voltohmmeter equipped with a pair of STX-2 chopstick electrodes (World Precision Instruments, Berlin, Germany) to verify the integrity of the cell monolayers for all experiments. TEER measurements were also carried out after the final timepoint of the permeability experiments to ensure that the cell monolayer integrity remained during the entire experiment. The TEER values were corrected to control wells containing culture medium alone (no cells) and normalized to the membrane surface area. The nanoparticles were added to the apical chambers at a polymer (R646 or R647) concentration of 180 μg mL^{-1} and a siRNA dose of either 10 or 60 nM. The siRNA molecules used in the experiment was fluorescently tagged with Cy5 to allow for monitoring of nanoparticle transport across the cell monolayer to the basolateral chamber at specific timepoints over 4 h. As controls, nanoparticles were added to transwells in which the membranes were precoated with collagen IV and fibronectin but without cell monolayers to measure the total transport across the porous filter membranes. The cumulative nanoparticle transport across the hBMEC monolayer was comparted to transport across the empty control inserts and the %-transported nanoparticles calculated at the specific timepoints. A Synergy 2 Multi-Mode Reader (BioTek Instruments, Winooski, VT, USA) was used to measure the fluorescent intensity in the basolateral chambers. The 24-well plates (Cellvis, Mountain View, CA, USA) used for the basolateral chambers had a black frame to only obtain fluorescent signal from the specific well. See ESI† for full details.

Characterization of nanoparticle transport *in vitro*

TEM was used to characterize the monolayer of hBMECs in the *in vitro* BBB model with and without exposure to nanoparticles in order to visualize the barrier properties, *i.e.* validation of tight junctions (TJs) and to evaluate mechanisms of nanoparticle crossing. As preparation of cross-sections for TEM characterization, the transwells containing a monolayer of hBMECs were first fixed with 3.0% formaldehyde and 1.5% glutaraldehyde in a 0.1 M cacodylate buffer, pH 7.4, at room temperature for one hour. Washing in 0.1 M cacodylate buffer was carried out for 15 min two times prior to post-fixation in Palade's 1% osmium tetroxide (OsO_4) for one hour on ice. A washing in Milli-Q H_2O was then applied for 15 min followed by further staining for 30 min using 1% tannic acid (Fisher Scientific) in 0.1 M cacodylate buffer. The samples were thereafter incubated overnight in Kellenberger solution, and subsequently rinsed once in Milli-Q H_2O and once in 50% ethanol. Dehydration was performed in graded series of ethanol (70%, 95%, and 100%), and then three washes in 100% ethanol prior to embedding in Epon. A diamond knife (Diatome, Hatfield, PA, USA) on a Leica Microtome (Leica Biosystems, Buffalo, IL, USA) was used to cut ultrathin (80 nm) sections. TEM imaging was carried out using a FEI Tecnai 12 TWIN TEM (FEI) microscope operated at 120 kV.

In vitro siRNA delivery to patient-derived glioblastoma cells

To analyse the ability of the nanoparticle formulations to cause functional siRNA-mediated knockdown, we utilized Allstars Human Cell death siRNA, which is a blend of siRNA molecules targeting genes essential for cell survival. For control experiments, we used replicate nanoparticle formulations that contained scrambled siRNA (scRNA) instead. To analyse non-specific nanoparticle-mediated cytotoxicity, cell death caused by exposure to nanoparticles containing the non-coding scrambled scRNA was compared to untreated control. In the initial experiment, the transfection efficiency of the formed nanoparticles loaded with 10, 60, or 120 nM of siRNA was examined to a patient-derived glioblastoma cell line GBM 612 which more closely recapitulates the human disease.[43–46] In the second setup, transwells seeded with hBMECs as described above was included, and in the basolateral compartments were GBM 612 cells cultured in order to examine the siRNA knockdown in the GBM cells provided by the nanoparticles being transported across the hBMEC barrier. The GBM 612 cells were cultured in a separate plate to avoid influencing the properties of the hBMEC monolayers. Right before the start of the experiment, the inserts with the hBMEC monolayers were moved to the plate with GBM 612 cells and the culture medium was replaced. In both methods, the incubation with the nanoparticles proceeded for 2 h at 37 °C, after which the medium with the nanoparticles was replaced with fresh culture medium. After three days, the GBM 612 cells were fixed and DAPI stained. To determine the cell death-mediated by the death siRNA molecules, the wells with GBM 612 cells exposed to nanoparticles loaded with siRNA were normalized to its counterpart loaded with scRNA. The toxicity was revealed by normalizing nanoparticles with scRNA-treated cells to cells only exposed to culture media. See ESI† for details.

Animals

Male nude athymic mice (Taconic Biosciences, Rensselaer, NY, USA) and male BALB/c (The Jackson Laboratory, Bar Harbor, ME, USA), each weighing about 30 g, were housed in standard facilities and were supplied with *ad libitum* access to food and water. All animal studies were performed in strict accordance with the NIH guidelines for the care and use of laboratory animals (NIH Publication no. 85-23 Rev. 1985). The animal experimental protocol used was approved by the Institutional Animal Care and Use Committees (IACUC) of the Johns Hopkins University. The animals were treated according to the policies and guidelines of the Johns Hopkins University Animal Care and Use Committee.

Inoculation of brain tumor cells for *in vivo* studies

For the surgical implantation of cannulas, the animals were anesthetized using a ketamine hydrochloride (Ketathesia, Butler Animal Health Supply, Dublin, OH, USA) solution followed by a scalp incision to expose the skull. A stereotactic frame was used to locate the position 1.5 mm interaural and 1.34 mm anterior to the bregma. The cannulas were inserted into this position for cells to be inoculated at a depth of 3.5 mm to the striatum of the mouse brain. Glue was first added beneath the mesh around the cannula to ensure its location, the incision was subsequently closed with surgical sutures. After one week of healing, 5×10^5 GBM1A cells was inoculated into each mouse following previously reported surgical procedures.[43,47] Tumor formation proceed for 12 days prior to the nanoparticle administration. All surgical procedures were carried out using standard sterile techniques.

Analysis of *in vivo* nanoparticle biodistribution and pharmacokinetics

In the biodistribution and pharmacokinetics studies for the engineered nanoparticle formulation, we used siRNA labelled with IR fluorescent dye (IRDye800CW; Integrated DNA Technologies, Coralville, IA, USA). In the biodistribution study, the nanoparticles were administrated *via* intravenous (IV) injections ($n = 4$) and we also had a control group ($n = 3$) included without nanoparticle treatments to analyze the contribution of auto-fluorescence of the organs. After 24 h post-administration, the animals were euthanized and dissection performed to harvest the organs for characterization. Imaging were carried out using both IVIS (PerkinElmer, Waltham, MA, USA) and LI-COR Pearl Impulse imager (LI-COR, Lincoln, NE, USA) to analyze the biodistribution of the nanoparticles. The acquired IVIS images were analyzed in Living Image software (PerkinElmer) and the LI-COR images with ImageJ (National Institutes of Health). In the pharmacokinetics study, the nanoparticles were administrated *via* IV injections ($n = 5$). At specific timepoints, retro-orbital blood draw was performed. LI-COR imaging was carried out to characterize the intensity of the IR-labelled nanoparticles and ImageJ was used for analysis.

In vivo blood–brain barrier integrity

We examined whether the nanoparticles influenced the BBB integrity using sodium fluorescein (Sigma-Aldrich) as a tracer. The BBB integrity was compared between animals that were treated with nanoparticles *via* intravenous injection *vs.* no nanoparticle treatment as controls ($n = 5$). Two hours post-NP administration, we injected 200 µL sodium fluorescein (7 mg mL^{-1}) intravenously and it was allowed to circulate for 1 h. We then performed a retro-orbital blood draw and perfused the animals with PBS. Thereafter, we harvested the brains and the tissue was homogenized and lysed in Liberase™ (Roche Diagnostics, Indianapolis, USA) at 80 µg mL^{-1} for 1 h at 37 °C, and subsequently centrifuged at 300 rcf for 5 min. The collected blood was centrifuged at 1500 rcf, for 15 min at 4 °C. The sodium fluorescein concentration of both the brain tissue and of the blood for each animal was analysed using a microplate reader Synergy 2 (485/20 nm and 528/20 nm) and Gen5 software (Biotek). We normalized the tissue fluorescence to the plasma fluorescence in each mouse.

Brain tumor accumulation of nanoparticles

For the accumulation study in the brain tumours, the siRNA was fluorescently labelled with Cy5 using Label IT Tracker kit (Mirus Bio LLC, Madison, WI, USA) to enable localization of nanoparticles. The nanoparticles were administrated either by intravenous (IV), intracardiac (IC), or intratumoral (IT) injections. After the animals were euthanized, we perfused them with 4% paraformaldehyde and the brains were extracted and post-fixed also in 4% paraformaldehyde for 2 h. The fixed brains were then kept in 30% sucrose in PBS until they did sink, which occurred after about three days. The brains were then embedded in Optimal Cutting Temperature compound (OCT; Electron Microscopy Sciences) and stored at −80 °C until use. A Leica CM3050 S cryostat (Leica Biosystems) was used to cryosection the brains and the prepared 20 µm thin sections were mounted onto glass slides. Fluorescent microscopy of brain cross-sections was carried out to visualize the GFP signal expressed by the glioblastoma cells and the Cy5-labeled nanoparticles. The GFP signal of the GBM cells were used to image the tumour area and the Cy5 signal was used to image the nanoparticles. The fluorescent microscopy images were acquired at 2.5× and 10× magnification using a Zeiss Axio Observer A1 (Zeiss, Jena, Germany) microscope equipped with a Zeiss Axiocam MRm camera using the AxioVision Release 4.8.2 software. ImageJ was used to measure the nanoparticle coverage within the tumor volumes. Images across the tumor volume of the brains were included for each animal. Brain sections for animals treated with nanoparticles without fluorescent labelling was used as control to ensure that no background noise was detected for the Cy5 signal.

Analysis of siRNA-mediated knockdown in brain tumors in vivo

In the experiment analyzing siRNA-mediated knockdown, IVIS imaging was performed to analyse the bioluminescence signal from the GBM1A cells expressing luciferase. IVIS imaging was performed before and after the nanoparticle administration and intraperitoneal injections (IP) of ᴅ-Luciferin Firefly (PerkinElmer) were performed according to manufacturer's protocol prior to each measurement. Image analysis was carried out using Living Image software. IVIS images of the bioluminescence signal for all animals were recorded first prior to nanoparticle injections (Day 0) and then each day to follow the bioluminescence signal from the GBM1A cells as a function of time.

The nanoparticles were loaded with either siRNA targeting firefly luciferase (Luc-siRNA) or negative control siRNA (scRNA) to allow for an optical readout whether successful delivery and luciferase knockdown was achieved.

Systemic toxicity study in vivo

We examined whether the systemically delivered nanoparticles caused any toxicity. Nanoparticles were administrated *via* IV injections and compared to animals without any treatment ($n = 3$). To analyse whether there was any acute response to the treatment, we performed blood analysis 48 h post-administration. We carried out alanine aminotransferase (ALT) and aspartate aminotransferase (AST) activity assays (Sigma-Aldrich), which are two important hepatic indicators. Blood serum was collected after centrifuged at 1500 rcf for 15 min at 4 °C and analysed according to supplier's protocol to determine the ALT and AST activities. Two weeks post-treatment, systemic toxicity was analysed by histopathological examinations of the harvested tissues. The tissue specimens were paraffin embedded, cut into 5 µm sections, and stained with hematoxylin/eosin (H&E) and then evaluated blinded by a pathologist.

Statistical analyses

All results are presented as mean ± standard error of the mean (SEM). All the statistical analyses were performed using Prism software (Graphpad Prism, San Diego, CA, USA) and in all the tests was $p < 0.05$ considered statistical significant. For the analysis of the *in vitro* transendothelial transport of the engineered nanoparticles, one-way ANOVA followed by Tukey's *post hoc* test was used to compare the total nanoparticle crossing after 4 h. For analysis of the *in vivo* biodistribution, a two-tailed Student's *t*-test was used to compare the IR-intensity of harvested organs between nanoparticle treatment and the control group. For analysis of the *in vivo* BBB integrity, a two-tailed Student's *t*-test was used to compare the normalized sodium fluorescein intensity between nanoparticle treatment and the control group. For the analysis of the nanoparticle coverage within the tumour volume in the *in vivo* study, one-way ANOVA was used to compare the different administration routes. For the analysis of the optical readout carried out with IVIS imaging in the first *in vivo* study, two-way ANOVA followed by Dunnett's post-test was used to compare the bioluminescence signal between the groups treated with nanoparticles injected *via* different administration routes at the different timepoints. For the analysis of the optical readout in the second *in vivo* study, analysed as normalized bioluminescence signal at Day 2 compared to Day 0 for each animal, a two-tailed Student's *t*-test was used to compare the
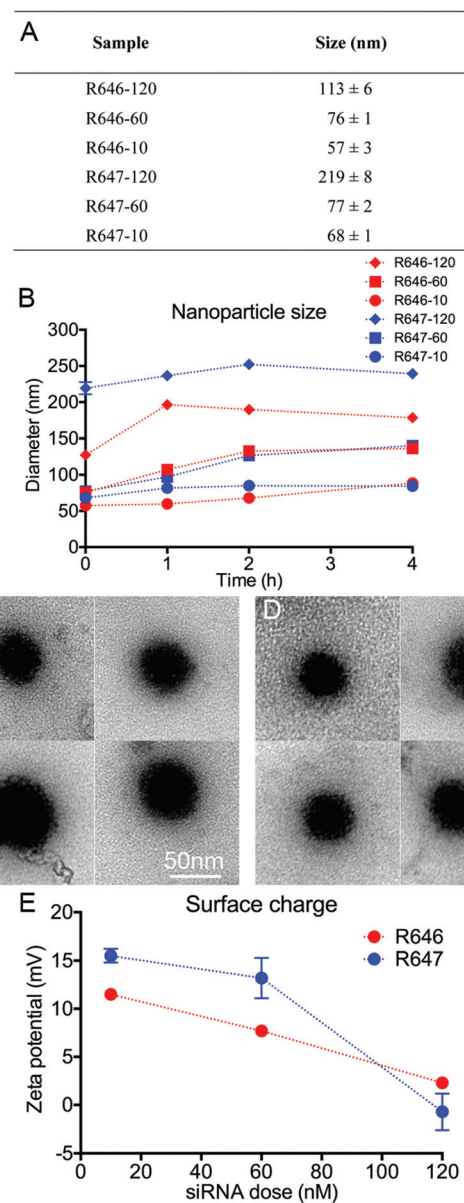
bioluminescence signal for the treatment group of nano-particles loaded with siRNA to the control group loaded with scRNA. For analysis of the systemic toxicity *in vivo*, a two-tailed Student's *t*-test was used to compare the ALT and AST activity in serum between nanoparticle treatment and the control group.

Results and discussion

Successful systemic *in vivo* delivery of siRNA to brain tumours using PBAEs, including BBB crossing, has not previously been demonstrated to our knowledge. In this study, we explored whether we could engineer nanoparticles with physical properties to enable this goal. PBAE polymers are biodegradable with a half-life in aqueous conditions ranging from approximately 2–6 h due to the presence of ester bonds in their backbone structure.[48] The hydrolysis of the ester bonds is beneficial by reducing the potential toxicity of PBAE polymers. While this allows relatively slow release, we sought to enable an immediate triggered release of siRNA as soon as the nanoparticles reach the intracellular environment of the reducing cytosol. Thus, we incorporated disulfide bonds into the PBAE structure for a triggered intracellular release of siRNA and to reduce potential cytotoxicity. Fig. 1 depicts the polymer synthesis for polymers R646 and R647, in which the backbone monomer 2,2′-disulfanediyl-bis(ethane-2,1-diyl) (BR6) was first polymerized with side chain monomer 4-amino-1-butanol (S4). This base polymer was then end-capped either with 2-((3-aminopropyl)amino)ethane-1-ol (E6) or 1-(3-aminopropyl)-4-methylpiperazine (E7) to form R646 or R647, respectively. These two polymer structures are promising for siRNA delivery to patient-derived glioblastoma cells over healthy neural progenitor cells *in vitro*.[38] In this study, we aimed to engineer bioreducible PBAE-siRNA nanoparticles for systemic delivery of siRNA *in vivo* to brain tumours by using an *in vitro* assay that mimic the BBB endothelium.

Physical properties of the PBAE-siRNA nanoparticles

Key features to achieve therapeutic efficacy upon systemic administration for nanoscale drug delivery systems are particle size and surface charge, since these physiological properties influence circulation time, tissue extravasation from the blood stream, tissue diffusion, and cellular uptake.[49] DLS was carried out to measure the diameter of the nanoparticles composed of either polymer R646 or R647 used as nanocarriers to encapsulate 10 (R64X-10), 60 (R64X-60), and 120 nM (R64X-120) of siRNA when incubated in medium containing 10% serum (FBS). The DLS results presented in Fig. 2A showed that a decreased nanoparticle diameter was obtained with a reduced siRNA dose, where the formulation R646-10 had a mean hydrodynamic diameter of 57 nm. DLS measurements were also carried out for nanoparticles incubated in medium with 10% serum at multiple timepoints over four hours. The results as shown in Fig. 2B demonstrate that the both the R646 and R647 nanoparticles had a low degree of aggregation in the presence of serum proteins over time. Furthermore, we performed TEM imaging to verify the DLS result of the particle

Sample	Size (nm)
R646-120	113 ± 6
R646-60	76 ± 1
R646-10	57 ± 3
R647-120	219 ± 8
R647-60	77 ± 2
R647-10	68 ± 1

Fig. 2 Characterization of nanoparticle (NP) size and surface charge when using either R646 or R647 polymers to encapsulate different doses of siRNA (10, 60, or 120 nM). (A) The DLS measurements showed that the nanoparticle size decreased when the siRNA dose was reduced (n = 3). (B) DLS measurements over 4 hours showed that the nanoparticles incubated in culture medium containing 10% serum had a low degree of aggregation (n = 3). (C and D) Representative TEM images of R646-10 and R647-10 NPs, respectively. (E) The surface charge of the nanoparticles decreased as a function of siRNA dose (n = 3). The error bars correspond to standard error of the mean (SEM).

sizing for the nanoparticles loaded with 10 nM siRNA and representative images are shown in Fig. 2C (R646-10) and Fig. 2D (R647-10). The TEM images were analysed using ImageJ to measure the nanoparticle diameters for R646-10 and R647-10 and the average diameters were 54 ± 2 nm and 59 ± 2 nm (mean ± SEM; $n \geq 20$), respectively, in good agreement with the DLS measurements.

Zeta potential measurements were carried out to examine the surface charge of the nanoparticles. When incubated in PBS (Fig. 2E), the surface charge decreased with increased siRNA loading at fixed polymer concentration, showing that the most positively charged nanoparticles were those with the smallest amount of siRNA (10 nM). The surface charge of the nanoparticles was also analysed in medium containing 10% serum proteins, in which case all of the nanoparticles had a negative zeta potential of approximately −8 mV, which indicates that anionic serum proteins assembled around the nanoparticles. However as seen in Fig. 2B, the protein assembly did not cause any major nanoparticle aggregation during the time period of 4 h.

The gel electrophoresis assay was performed to examine nanoparticle stability when the particles were incubated in PBS, in culture medium containing 10% serum, or in a microenvironment that mimics the intracellular cytosol (5 mM GSH). Fig. 3A–C shows the results for the nanoparticles with polymer/siRNA weight/weight (w/w) ratios of 1200 w/w, 200 w/w, and 100 w/w which corresponds to loading of 10, 60, and 120 nM siRNA respectively. It was observed at the 0 h timepoint that in both PBS and 10% serum-containing medium the siRNA was completely encapsulated in all of the R646 and R647 nanoparticle formulations. When incubated in PBS over time, most of the siRNA was held in the nanoparticles, but the nanoparticles also started to show release at 2 h for the 100 w/w formulations and at 4 h for the 200 w/w formulations, whereas no release of siRNA did occur over 4 h for the 1200 w/w formulations. When 10% serum was present, only the

1200 w/w formulations were able to completely encapsulate the siRNA load across all time points. A low siRNA release occurred in 10% serum with the 200 w/w R646 nanoparticles at 4 h and the 100 w/w R646 nanoparticles at 2 h and 4 h. Similarly, a minor siRNA release was observed in 10% serum for both the 200 w/w and 100 w/w R647 formulations at 2 h and 4 h. Thus, the R646 polymer was able to bind siRNA slightly better than the R647 polymer since at 200 w/w the R646-siRNA nanoparticles exhibited no release at 2 h. Nanoparticles were also incubated in 5 mM GSH to mimic the cytosolic environment and hence evaluate the potential triggered intracellular release of siRNA. Both the R646 and R647 nanoparticles across all w/w formulations had efficient siRNA release in the cytosol mimicking environment including the early 15 min timepoint, indicating environmentally-triggered release. Combined, the results from the gel electrophoresis assay demonstrate that a higher polymer to siRNA weight ratio than 100 w/w is needed for the nanoparticle compositions to have good stability during circulation as the presence of serum proteins influence the siRNA encapsulation at lower polymer ratios, with the 1200 w/w formulations showing the strongest stability among those tested.

NTA was carried out to evaluate the nanoparticle concentration and the amount of siRNA molecules loaded into each particle. The nanoparticle concentration was approximately constant at 7×10^{10} nanoparticles per mL for all of the different polymer-siRNA compositions evaluated. The number of siRNA molecules encapsulated into each nanoparticle was found to increase approximately linearly as a function of the siRNA dose used in the formulations, as shown in Fig. 3D.
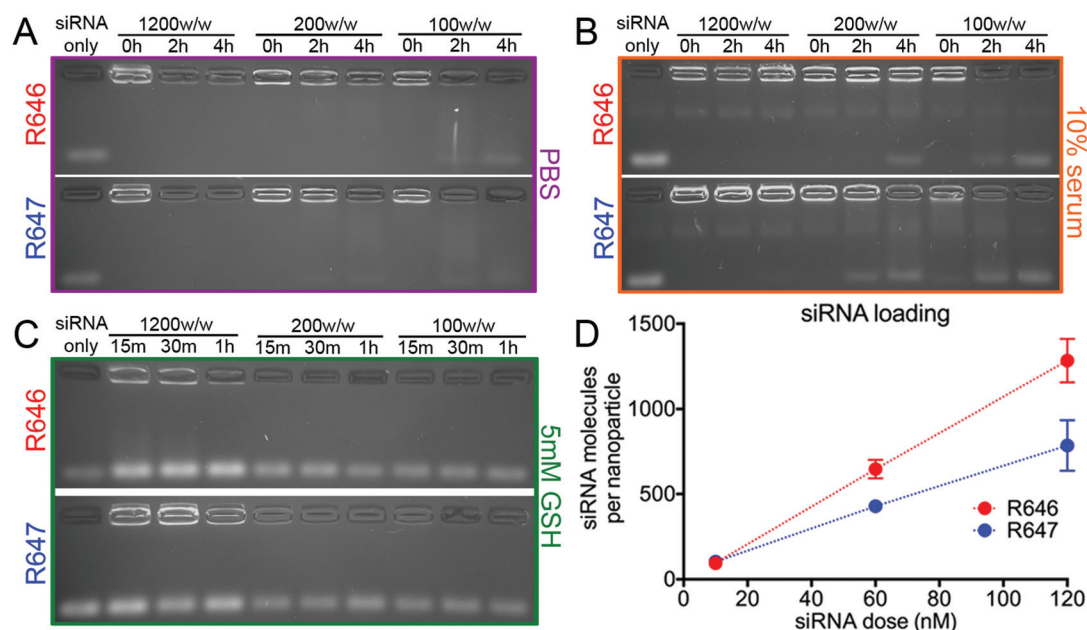
Fig. 3 Characterization of nanoparticle (NP) encapsulation stability and siRNA loading. (A) The gel electrophoresis assay showed that the nanoparticles held most of the siRNA when incubated in PBS over time, as only minor dissociation was observed for the 200 w/w and 100 w/w formulations. (B) In 10% serum, it was only the 1200 w/w formulations that completely bound the siRNA load throughout 4 h. (C) In the cytosol mimicking environment (5 mM GSH), all formulations released their siRNA load within 15 min. (D) Nanoparticle tracking analysis (NTA) demonstrating the siRNA loading in each nanoparticle. The error bars correspond to standard error of the mean (SEM).

Together, we demonstrated both the size and charge can be tuned by adjusting the mass ratio in between the cationic polymer and the anionic siRNA load. Moreover, a positive surface charge may trigger crossing of biological barriers such as the BBB *via* an adsorptive mediated mechanism. Despite a positive charge for our nanoparticle formulations, they still demonstrated good stability (4 h) when incubated in presence of serum, as shown in Fig. 2B. The presence of serum proteins may also influence the encapsulation stability of the siRNA load. By gel electrophoresis, we demonstrated that a high ratio of polymer to siRNA load is needed to ensure a high colloidal stability and thereby prevent siRNA dissociation upon systemic administration. In addition, the cationic charge provided by the endcapping group also contributed to the encapsulation efficiency. We observed in the gel electrophoresis assay that the polymer R646 had more efficient encapsulation of siRNA than R647, which is likely due to the E6 endcap monomer having an additional secondary amine compared to E7, leading to increased electrostatic interactions with the siRNA payload (Fig. 1). Moreover, a higher polymer mass ratio didn't reduce the siRNA release rate in intracellular environment, due to the triggered release by the presence of disulfide bonds in the polymer structure that quickly degrade the multivalent cationic polymer structure in the cytosol.

Transendothelial nanoparticle transport in an *in vitro* blood–brain barrier model

To screen for an optimized nanoparticle formulation and to understand the mechanism for transendothelial transport of the particles, a transwell model was used that mimics the BBB endothelium, as illustrated in Fig. 4A. A recently developed *in vitro* BBB model was utilized, in which iPSC-derived human brain microvascular endothelial cells (dhBMECs) were seeded as a monolayer in transwells.[39,40] To ensure monolayer formation, we thoroughly dispersed the cells prior to seeding. The cell seeding density is also critical in order to avoid non-adherent cells, herein we seeded 1×10^6 cells per mL on the inserts coated with a mixture of collagen IV and fibronectin

and waited two days to obtain good monolayer integrity. Katt and coworkers have demonstrated that the iPSC differentiated hBMEC monolayers express the TJ proteins ZO-1, occludin, and claudin-5 in the cell junctions of BC1 iPSC-derived hBMEC monolayers.[40,50] Further, the authors also demonstrated that the hBMECs expressed the platelet endothelial cell adhesion molecule PECAM-1, the glucose transport GLUT-1, and the efflux pump protein Poly-glycoprotein (P-gp).[40,50] This protein expression profile replicates features that are characteristics for the BBB endothelium. In addition, the authors showed that Lucifer yellow permeability of the hBMEC monolayers was approximately 4×10^{-7} cm s^{-1}. Monolayers with a Lucifer yellow permeability below 1×10^{-6} cm s^{-1} are considered to have restricted paracellular transport.[51] The ability of nanoparticle formulations loaded with 10 or 60 nM siRNA at achieving transendothelial transport across the dhBMEC monolayers (average TEER was 498 Ω cm^2) was analysed. Nanoparticle R646-10 was the formulation that exhibited the highest rate of transport across the dhBMEC monolayer as shown in Fig. 4B, with 2 to 10-fold increased permeability compared to the other nanoparticles formulations across all time points evaluated. After 4 h, the total nanoparticle crossing was statistically higher for R646-10 compared to R646-60 and R647-10 ($p < 0.05$; $n = 3$–5).

To explore the mechanism of the nanoparticle uptake and transport across the monolayer, ultrastructural TEM characterization was performed (Fig. 5A). In the acquired TEM images, the presence of adherens junctions (AJs) in between adjacent endothelial cells were observed, as shown in Fig. 5B and C. Moreover, Fig. 5D–G demonstrate nanoparticle transport across the dhBMEC monolayer at different cross-sectional locations. Fig. 5D shows two nanoparticles that have adsorbed to the cellular membrane, and around them are endocytic pits (EPs) formed to promote uptake. The nanoparticles are thereafter transported in vesicles (Vs) as shown in Fig. 5E–G, where Fig. 5E shows a location close to the apical side, Fig. 5F in the middle of the monolayer, and Fig. 5G close to basolateral side.

The presence of AJs shown by electron microscopy and the TEER values of about 500 Ω cm^2 for the assay we used with BMECs derived from iPSCs show good recapitulation to the properties of the BBB endothelium. Moreover, the TEM images suggest that the engineered nanoparticles are able to cross *via* a vesicular mechanism. This is likely due to the physical properties of the nanoparticles, including the cationic charge of the polymeric nanoparticles and their small size, allowing them to adsorb to the negatively charged surface of the BBB endothelium, and thereby trigger adsorptive-mediated transcytosis.[28]

In vitro delivery of siRNA to patient-derived glioblastoma cells using bioreducible PBAE nanoparticles

The siRNA delivery efficacy to patient-derived GBM cells for the different nanoparticle formulations using either R646 or R647 polymer with varied doses of siRNA is presented in Fig. 6. In the test group, we used nanoparticles containing cell death-siRNA, which is a blend of siRNAs targeting genes essential for cell survival and as control group, nanoparticles con-
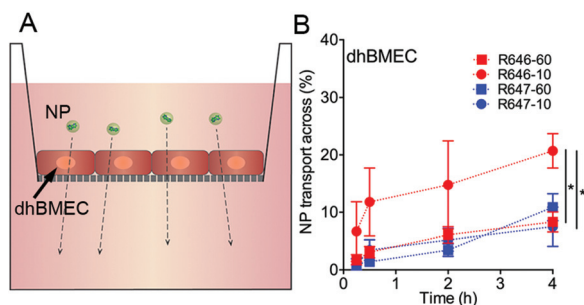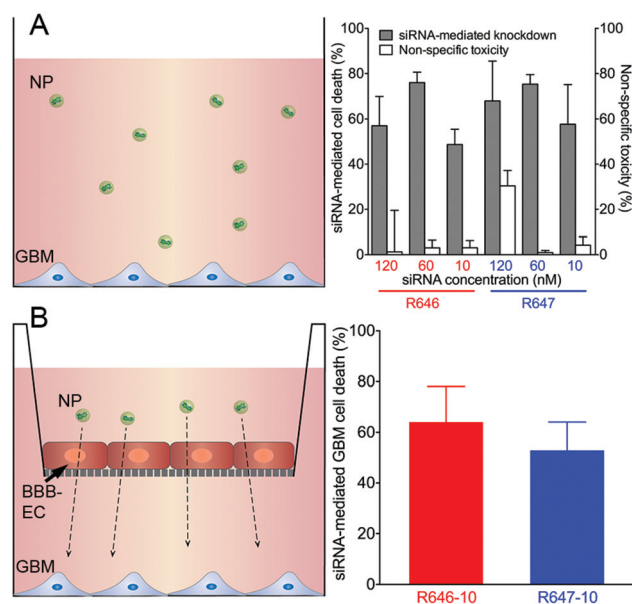

Fig. 4 *In vitro* transendothelial transport of the engineered nanoparticles (NPs). (A) Schematic illustration of the transwell setup used to analyze NP transport across an iPSC-derived human brain microvascular endothelial cell (dhBMEC) monolayer. (B) The formulation with R646 and 10 nM siRNA dose (R646-10) achieved the most efficient crossing of the dhBMEC monolayers. The error bars correspond to standard error of the mean (SEM; *n* = 3–5).
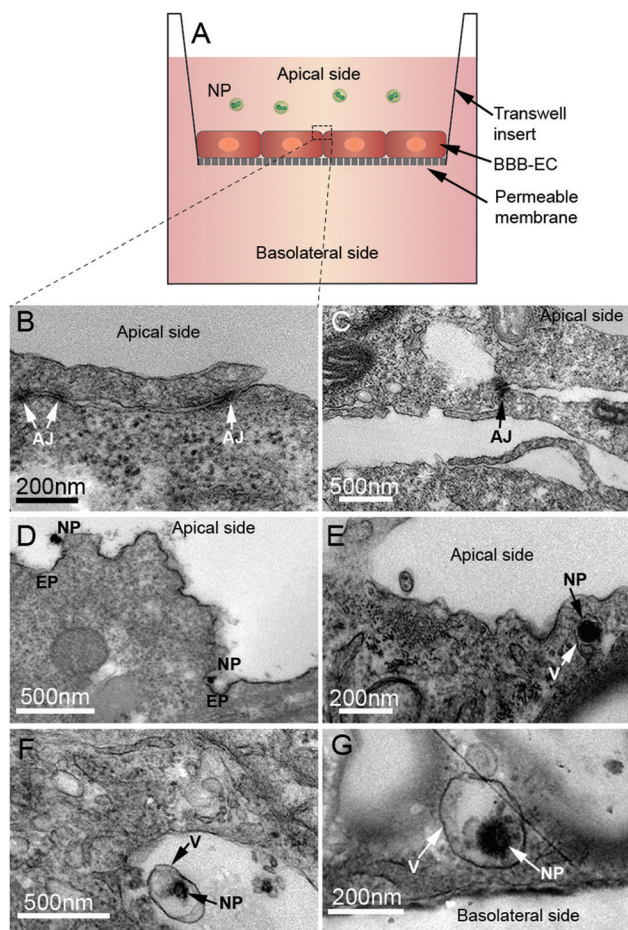
Fig. 5 TEM characterization was used to examine the presence of adherens junctions (AJs) between endothelial cells (ECs) and the mechanism of the transendothelial nanoparticle (NP) transport. (A) A schematic of the *in vitro* assay to illustrate a TEM specimen taken from the blood–brain barrier endothelium (BBB-EC). (B and C) TEM images showing that AJs were present in between adjacent ECs in the *in vitro* assay. (D) Cellular uptake of NPs by endocytic pits (EPs). (E–G) NPs being transported inside vesicles (V) close to the apical side (E), in the middle of the endothelium (F), and close to the basolateral compartment (G).

Fig. 6 siRNA delivery to patient-derived glioblastoma cells (GBM). (A) All nanoparticle (NP) formulations provided an efficient siRNA-mediated cell death of the GBM cells when seeded in culture plates. (B) Both the R646-10 and R647-10 NPs achieved siRNA-mediated cell death of the GBM cells following transvascularization of the monolayer mimicking the blood–brain barrier endothelium (BBB-EC). The error bars correspond to standard error of the mean (SEM; n = 3).

PBAE/siRNA nanoparticle biodistribution and pharmacokinetics *in vivo*

An orthotopic glioblastoma model that utilized human patient-derived GBM cells (GBM1A) implanted intracranially in mice was used to evaluate the siRNA-containing nanoparticles. This *in vivo* model using primary glioblastoma cells recapitulates the human disease.[35,43,47] For the *in vivo* studies, GFP + Luc + patient-derived GBM cells were inoculated so that the brain cancer cells could be visualized by both fluorescence and bioluminescence. The nanoparticle formulation R646-10 that demonstrated the highest permeability in the *in vitro* BBB model among the analysed formulations was tested *in vivo* in the orthotopic glioblastoma to examine whether it could provide systemic siRNA delivery to brain tumours. We used siRNA labelled with an IR-fluorescent dye to analyse the biodistribution of the nanoparticle formulation. As shown in Fig. 7A–C, after 24 h the nanoparticles showed no accumulation in any of the organs except for the brain, which showed a statistically higher signal for the nanoparticle treatment compared to the control (p = 0.0073; n = 3–4). The background signal observed is due to autofluorescence caused by the presence of chlorophyll in the mouse diet. We further analysed the pharmacokinetics of the R646-10 nanoparticle formulation after IV administration (n = 5). We used IR-labelled siRNA in the nanoparticle formulation and collected blood at specific timepoints. As shown in Fig. 7D, the blood clearance half-life of the nanoparticles is approximately 10 minutes. To analyse whether IV administration of engineered nanoparticle formulation influenced the BBB integrity, we
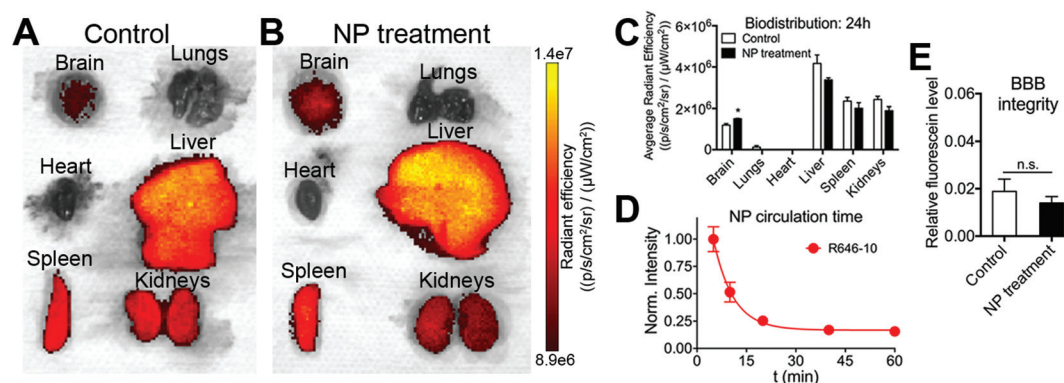
taining scrambled siRNA was used. Fig. 6A shows transfection of the GBM cells where all nanoparticle formulations were found to be effective, generating knockdown to cause siRNA-mediated cell death in 50–80% of the human glioblastoma cells. Nonspecific cytotoxicity caused by the nanoparticles delivering scrambled siRNA was negligible, except for the R647-120 formulation. R646-10 and R647-10 were further analysed for knockdown of the GBM cells with the addition of the *in vitro* BBB model using a dhBMEC monolayer. In this experimental set-up (Fig. 6B), the GBM cells were cultured in the basolateral chambers to evaluate siRNA delivery efficacy for the nanoparticles that crossed the dhBMEC layer. As shown in Fig. 6B, both R646-10 and R647-10 generated significant siRNA-mediated knockdown in about 50% of the GBM cells following transendothelial transport.

Fig. 7 (A–C) *In vivo* biodistribution for the R646-10 nanoparticle (NP)-siRNA formulation 24 h post intravenous injections (*n* = 3–4). Representative IVIS images for IR intensity of the retrieved organs from a control (A) and for an animal with NP treatment (B). (C) A statistically higher IR intensity was observed in the brains for the animals with NP treatment compared to controls. (D) A pharmacokinetics study was performed to determine the circulation time of the R646-10 NP formulation after intravenous injection (*n* = 5). (E) R646-10 NPs do not influence the blood–brain barrier (BBB) integrity. Intravenously administered sodium fluorescein does not more easily cross the BBB in mice that received intravenously injected R646-10 NPs compared to untreated controls (*n* = 5). The error bars correspond to standard error of the mean (SEM).

injected sodium fluorescein IV and measured extravasation to the brain 1 h later. Fig. 7E shows the fluorescein signal in the brains normalized to the signal in blood serum. The relative fluorescein level in the brains was similar between animals that received IV injected R646-10 nanoparticles compared to untreated animals ($p = 0.46$; $n = 5$). This result indicates that the nanoparticle formulation did not influence the BBB integrity.

PBAE/siRNA nanoparticle accumulation in orthotopic human brain tumours *in vivo*

Fluorescence microscopy was performed to characterize the distribution in the brain tissue of the Cy5-labeled siRNA-containing nanoparticles that either were administrated systemically *via* IV or IC injections, or locally *via* IT injections. Representative images for the different groups are presented in Fig. 8A, in which the GFP signal shows the tumour region and the Cy5 signal the siRNA-containing nanoparticles. Locally administrated nanoparticles without Cy5-labeling was included as a control group. It was observed that the nanoparticles were capable of accumulating in the brain tumours following systemic administration (IV and IC). We quantified the extent to which the Cy5-labeled nanoparticles co-localized with the GFP + tumours following the three administration methods: IV, IC, and IT (local) injections. As shown in Fig. 8B, the nanoparticle coverage of the tumour volumes was above 30% for all of the groups. Interestingly, the nanoparticle group that was administered IV was similar to the nanoparticle group administered IT. Taken together, the biodistribution study and the fluorescence microscopy of the brain tumours demonstrated that the nanoparticles could reach the brain following systemic administration as inferred from the *in vitro* BBB model. Interestingly, as shown in Fig. 8B, the systemically (IV) administered nanoparticles can in some cases reach wider regions of a brain tumour than the locally delivered (IT) nanoparticles, presumably due to diffusion limited transport in the vicinity of the cannula for IT delivery. The engineered bioreducible nanoparticles likely reached the

tumours through active transport across the BBB *via* transcytosis by a vesicular mechanism as observed in our *in vitro* experiments (Fig. 5D–G). In addition, there may be abnormalities in the endothelium in the vicinity of the tumour which can improve nanoparticle transport across the BBB. For example, an increased vessel wall thickness is a common feature of the glioma vasculature, leading to increased non-selective transendothelial transport.[52,53] It has also been reported that in glioma there is an increase in the size and numbers of cytoplasmic vesicles including caveolae and vesicular vacuolar organelles (VVO).[54]

***In vivo* siRNA delivery to glioblastoma tumours using bioreducible nanoparticles**

The inoculated GBM cells expressed luciferase and thus R646-10 nanoparticles were loaded with either siRNA targeting the bioluminescence expression or scRNA as control to allow for a non-invasive optical bioluminescent readout for *in vivo* knockdown activity. Two separate *in vivo* studies were performed to analyse the efficacy. In the first study, the nanoparticle formulation was administered both *via* systemic (IV and IC) and local (IT) injections as comparison. As shown in Fig. 8C, the NP-mediated siRNA delivery through all three routes, IV, IC, and IT caused a significant reduction in bioluminescence expression in the GBM cells compared to the control ($n = 3–4$). The reduction in bioluminescence was approximately the same for all three different administration routes, which is consistent with the equivalent tumour coverage observed with labelled nanoparticles administered *via* all three routes (Fig. 8B). Representative IVIS images for animals treated with siRNA *via* IV, IC, and IT administration and with scRNA as a control prior to nanoparticles injections and 2 days after treatment are shown in Fig. 8D. As all three administration routes performed similarly for efficacy with maximum knockdown within 2 days post treatment, we chose IV administration for our second *in vivo* study as the preferred route as it is the least invasive. A significantly reduced luciferase signal was found
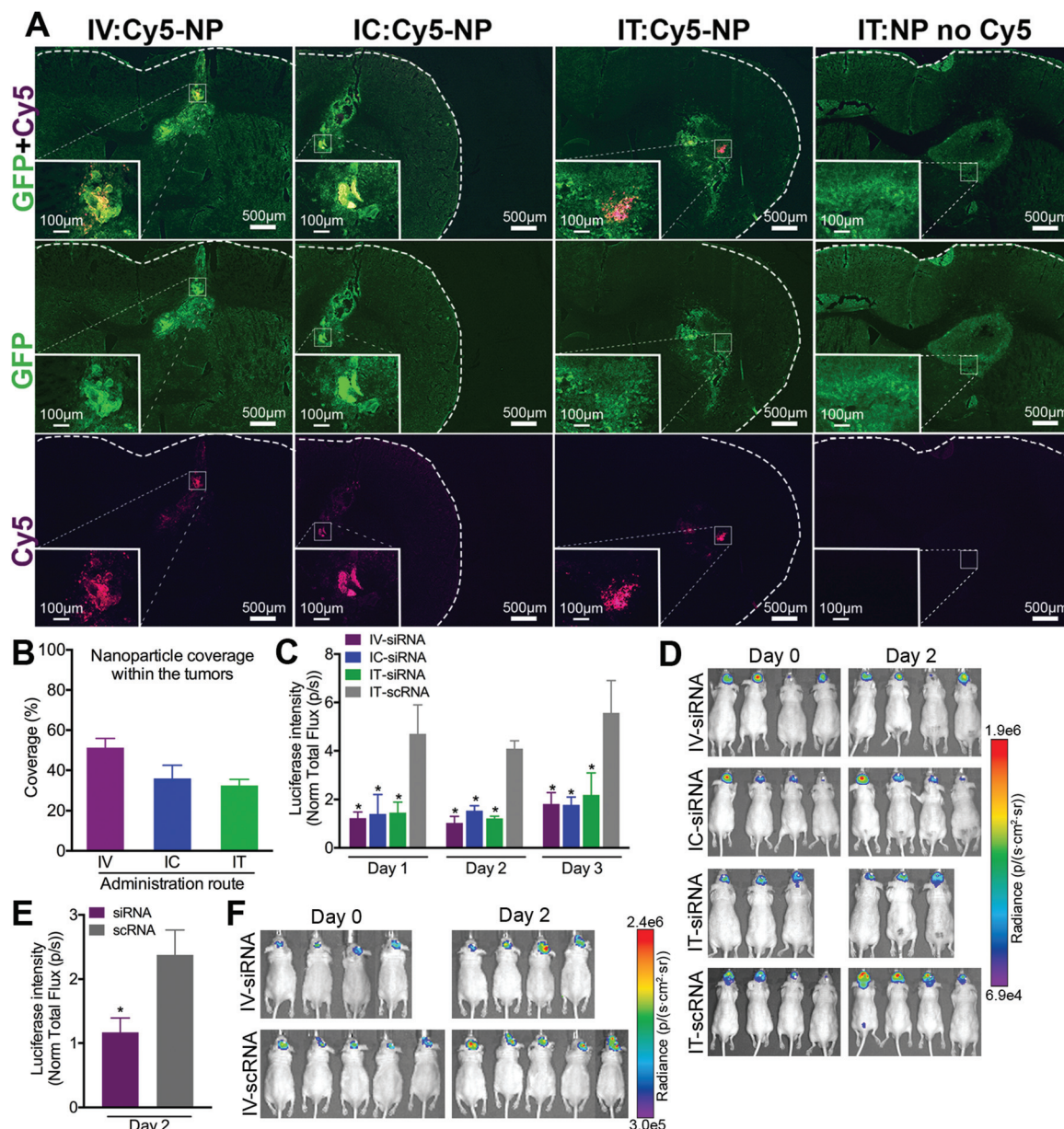
Fig. 8 Nanoparticle (NP)-mediated siRNA delivery to patient-derived glioblastoma (GBM) tumors *in vivo*. (A) R646-10 NPs were administrated either systemically by intravenous (IV) or intracardiac (IC) injections, or locally by intratumoral (IT) injections and the NP distributions through GFP + tumor regions were examined by measuring Cy5-labelled siRNA. (B) The NP coverage within the tumor volumes was similar after IV and IC administration compared to local IT delivery. (C) A significant reduction of bioluminescence signal of the Luc + brain tumors was found for all three administration routes of the siRNA-NPs compared to scRNA control NPs ($n = 3-4$). (D) IVIS images prior (Day 0) and two days (Day 2) after treatment for all administration routes (IV, IC, and IT) with siRNA-NPs and locally delivered (IT) scRNA-NPs. (E) A second *in vivo* study comparing IV administration of NPs encapsulating either siRNA or scRNA verified significant knockdown of GBM cells ($n = 4-5$). (F) IVIS images from second study prior (Day 0) and two days (Day 2) after treatment with siRNA-NP and scRNA-NP. The error bars correspond to standard error of the mean (SEM).

for R646-10 nanoparticles loaded with siRNA compared with scRNA loading ($p = 0.028$; $n = 4-5$) as shown in Fig. 8E. This result further verifies the finding from the initial *in vivo* study that the systemically delivered nanoparticles were able to provide significant knockdown in the inoculated patient-derived glioblastoma cells. In Fig. 8F, representative IVIS images of animals prior to nanoparticle administration and two days post injections are shown. The animals with scRNA

treatment (bottom row) displayed an increased bioluminescence which corresponds to the tumour growth over two days. Whereas, the animals treated with siRNA-Luc loaded nanoparticles (top row) had a relatively reduced level of bioluminescence compared to the increase for the controls. The R646-10 nanoparticle formulation provided systemic delivery of siRNA to brain tumours without causing any signs of systemic toxicity. No significant differences were observed for the

ALT ($p = 0.78$; $n = 3$) and the AST ($p = 0.87$; $n = 3$) activity in the blood serum 48 h post-treatment of IV administrated nanoparticles compared to control animals without treatment, as shown in Fig. S3.† This result indicates that the nanoparticle formulation does not show a significant risk of hepatoxicity. The tissues harvested two weeks post-administration of R646-10 nanoparticles for histopathology demonstrated no changes or abnormalities related to the nanoparticle treatment, including in the brain, heart, lungs, liver, spleen, and kidneys. Representative histopathological images of the analysed tissues are shown in Fig. S4† for both the treatment group with nanoparticle administration and the controls without treatment. Further, administration of the nanoparticles did not change the integrity of the BBB (Fig. 7E). No adverse side effects were observed in any of our animal studies. Thus in our studies, the R646-10 nanoparticle formulation led to safe delivery across the BBB to the brain *in vivo*. Taken, together, the ability of the engineered bioreducible polymeric nanoparticles to enable systemic delivery to the brain could open new avenues for safe and efficient siRNA delivery for improved brain cancer therapies as well as potential neuromodulation more generally.

Conclusions

In this study, we utilized an *in vitro* assay to mimic the brain microvascular endothelium to yield knowledge to engineer a bioreducible polymeric nanoparticle formulation that could enable blood–brain barrier (BBB) crossing and siRNA delivery to brain tumors *in vivo*. The bioreducible poly(β-amino ester) (PBAE)-based nanoparticle that had the highest *in vitro* permeability and provided siRNA-mediated knockdown to patient-derived glioblastoma cells had a positive surface charge, a particle diameter of approximately 57 nm, was stable in the presence of serum proteins, and efficiently released siRNA in a triggered fashion in a cytosol-mimicking environment. It was shown using TEM that the engineered bioreducible nanoparticles crossed the microvascular endothelium *via* transcytosis. The nanoparticle formulation with the highest *in vitro* transport was found to enter the brain following systemic intravenous administration in a mouse model of patient-derived glioblastoma. Moreover, the nanoparticles were able to knock-down a reporter gene within the human patient-derived glioblastoma cells in the orthotopic mouse model in a safe manner. Taken together, this research demonstrates new frontiers for engineering nanomedicines for transendothelial transport to the brain based on *in vitro* evaluation. The ability of the engineered bioreducible polymeric nanoparticles to enable safe and effective systemic delivery to the brain could potentially open new avenues for siRNA-based therapeutic treatments for brain cancer.

Conflicts of interest

There are no conflicts to declare.

Acknowledgements

References

1 F. B. Furnari, T. Fenton, R. M. Bachoo, A. Mukasa, J. M. Stommel, A. Stegh, W. C. Hahn, K. L. Ligon, D. N. Louis, C. Brennan, L. Chin, R. A. DePinho and W. K. Cavenee, *Genes Dev.*, 2007, **21**, 2683–2710.

2 M. J. McGirt, K. L. Chaichana, M. Gathinji, F. J. Attenello, K. Than, A. Olivi, J. D. Jon, D. Weingart, H. Brem and A. Quiñones-Hinojosa, *J. Neurosurg.*, 2009, **110**, 156–162.

3 P. Y. Wen and S. Kesari, *N. Engl. J. Med.*, 2008, **359**, 492–507.

4 A. D. Wong, M. Ye, A. F. Levy, J. D. Rothstein, D. E. Bergles and P. C. Searson, *Front. Neuroeng.*, 2013, **6**, 7.

5 N. J. Abbott, A. A. Patabendige, D. E. Dolman, S. R. Yusof and D. J. Begley, *Neurobiol. Dis.*, 2010, **37**, 13–25.

6 W. M. Pardridge, *Drug Discovery Today*, 2007, **12**, 54–61.

7 S. Sathornsumetee, J. N. Rich and D. A. Reardon, *Neurol. Clin.*, 2007, **25**, 1111–1139.

8 S. Sathornsumetee, D. A. Reardon, A. Desjardins, J. A. Quinn, J. J. Vredenburgh and J. N. Rich, *Cancer*, 2007, **110**, 13–24.

9 H. Mao, D. G. LeBrun, J. X. Yang, V. F. Zhu and M. Li, *Cancer Invest.*, 2012, **30**, 48–56.

10 R. Kanasty, J. R. Dorkin, A. Vegas and D. Anderson, *Nat. Mater.*, 2013, **12**, 967–977.

11 Y. K. Oh and T. G. Park, *Adv. Drug Delivery Rev.*, 2009, **61**, 850–862.

12 K. A. Whitehead, R. Langer and D. G. Anderson, *Nat. Rev. Drug Discovery*, 2009, **8**, 129–138.

13 D. W. Pack, A. S. Hoffman, S. Pun and P. S. Stayton, *Nat. Rev. Drug Discovery*, 2005, **4**, 581–593.

14 A. Akinc, A. Zumbuehl, M. Goldberg, E. S. Leshchiner, V. Busini, N. Hossain, S. A. Bacallado, D. N. Nguyen, J. Fuller, R. Alvarez, A. Borodovsky, T. Borland, R. Constien, A. de Fougerolles, J. R. Dorkin, K. N. Jayaprakash, M. Jayaraman, M. John, V. Koteliansky, M. Manoharan, L. Nechev, J. Qin, T. Racie, D. Raitcheva, K. G. Rajeev, D. W. Y. Sah, J. Soutschek, I. Toudjarska, H.-P. Vornlocher, T. S. Zimmermann, R. Langer and D. G. Anderson, *Nat. Biotechnol.*, 2008, **26**, 561–569.

15 S. C. Semple, A. Akinc, J. Chen, A. P. Sandhu, B. L. Mui, C. K. Cho, D. W. Y. Sah, D. Stebbing, E. J. Crosley, E. Yaworski, I. M. Hafez, J. R. Dorkin, J. Qin, K. Lam, K. G. Rajeev,

K. F. Wong, L. B. Jeffs, L. Nechev, M. L. Eisenhardt, M. Jayaraman, M. Kazem, M. A. Maier, M. Srinivasulu, M. J. Weinstein, Q. Chen, R. Alvarez, S. A. Barros, S. De, S. K. Klimuk, T. Borland, V. Kosovrasti, W. L. Cantley, Y. K. Tam, M. Manoharan, M. A. Ciufolini, M. A. Tracy, A. de Fougerolles, I. MacLachlan, P. R. Cullis, T. D. Madden and M. J. Hope, *Nat. Biotechnol.*, 2010, **28**, 172–176.

16 Y. Zhang, A. Satterlee and L. Huang, *Mol. Ther.*, 2012, **20**, 1298–1304.

17 T. S. Zimmermann, A. C. H. Lee, A. Akinc, B. Bramlage, D. Bumcrot, M. N. Fedoruk, J. Harborth, J. A. Heyes, L. B. Jeffs, M. John, A. D. Judge, K. Lam, K. McClintock, L. V. Nechev, L. R. Palmer, T. Racie, I. Rohl, S. Seiffert, S. Shanmugam, V. Sood, J. Soutschek, I. Toudjarska, A. J. Wheat, E. Yaworski, W. Zedalis, V. Koteliansky, M. Manoharan, H. P. Vornlocher and I. MacLachlan, *Nature*, 2006, **441**, 111–114.

18 A. M. Derfus, A. A. Chen, D. H. Min, E. Ruoslahti and S. N. Bhatia, *Bioconjugate Chem.*, 2007, **18**, 1391–1396.

19 A. Elbakry, A. Zaky, R. Liebkl, R. Rachel, A. Goepferich and M. Breunig, *Nano Lett.*, 2009, **9**, 2059–2064.

20 J. L. Shen, H. C. Kim, H. Su, F. Wang, J. Wolfram, D. Kirui, J. H. Mai, C. F. Mu, L. N. Ji, Z. W. Mao and H. F. Shen, *Theranostics*, 2014, **4**, 487–497.

21 T. A. Xia, M. Kovochich, M. Liong, H. Meng, S. Kabehie, S. George, J. I. Zink and A. E. Nel, *ACS Nano*, 2009, **3**, 3273–3286.

22 F. H. Meng, W. E. Hennink and Z. Zhong, *Biomaterials*, 2009, **30**, 2180–2198.

23 M. E. Davis, J. E. Zuckerman, C. H. J. Choi, D. Seligson, A. Tolcher, C. A. Alabi, Y. Yen, J. D. Heidel and A. Ribas, *Nature*, 2010, **464**, 1067–1071.

24 K. A. Woodrow, Y. Cu, C. J. Booth, J. K. Saucier-Sawyer, M. J. Wood and W. M. Saltzman, *Nat. Mater.*, 2009, **8**, 526–533.

25 A. Zintchenko, A. Philipp, A. Dehshahri and E. Wagner, *Bioconjugate Chem.*, 2008, **19**, 1448–1455.

26 F. Schlachetzki, Y. Zhang, R. J. Boado and W. M. Pardridge, *Neurology*, 2004, **62**, 1275–1281.

27 H. L. Wong, X. Y. Wu and R. Bendayan, *Adv. Drug Delivery Rev.*, 2012, **64**, 686–700.

28 Y. Chen and L. H. Liu, *Adv. Drug Delivery Rev.*, 2012, **64**, 640–665.

29 W. M. Pardridge, J. L. Buciak, Y. S. Kang and R. J. Boado, *J. Clin. Invest.*, 1993, **92**, 2224–2229.

30 F. Herve, N. Ghinea and J. M. Scherrmann, *AAPS J.*, 2008, **10**, 455–472.

31 A. Akinc, D. G. Anderson, D. M. Lynn and R. Langer, *Bioconjugate Chem.*, 2003, **14**, 979–988.

32 A. Akinc, D. M. Lynn, D. G. Anderson and R. Langer, *J. Am. Chem. Soc.*, 2003, **125**, 5316–5323.

33 D. G. Anderson, D. M. Lynn and R. Langer, *Angew. Chem., Int. Ed.*, 2003, **42**, 3153–3158.

34 J. J. Green, R. Langer and D. G. Anderson, *Acc. Chem. Res.*, 2008, **41**, 749–759.

35 H. Guerrero-Cazares, S. Y. Tzeng, N. P. Young, A. O. Abutaleb, A. Quinones-Hinojosa and J. J. Green, *ACS Nano*, 2014, **8**, 5141–5153.

36 J. Sunshine, J. J. Green, K. P. Mahon, F. Yang, A. A. Eltoukhy, D. N. Nguyen, R. Langer and D. G. Anderson, *Adv. Mater.*, 2009, **21**, 4947–4951.

37 S. Y. Tzeng and J. J. Green, *Adv. Healthcare Mater.*, 2013, **2**, 468–480.

38 K. L. Kozielski, S. Y. Tzeng, B. A. H. De Mendoza and J. J. Green, *ACS Nano*, 2014, **8**, 3232–3241.

39 E. S. Lippmann, S. M. Azarin, J. E. Kay, R. A. Nessler, H. K. Wilson, A. Al-Ahmad, S. P. Palecek and E. V. Shusta, *Nat. Biotechnol.*, 2012, **30**, 783–791.

40 M. E. Katt, Z. S. Xu, S. Gerecht and P. C. Searson, *PLoS One*, 2016, DOI: 10.1371/journal.pone.0152105.

41 N. S. Bhise, R. S. Gray, J. C. Sunshine, S. Htet, A. J. Ewald and J. J. Green, *Biomaterials*, 2010, **31**, 8088–8096.

42 E. S. Lippmann, A. Al-Ahmad, S. M. Azarin, S. P. Palecek and E. V. Shusta, *Sci. Rep.*, 2014, DOI: 10.1038/srep04160.

43 M. Ying, J. Tilghman, Y. Wei, H. Guerrero-Cazares, A. Quinones-Hinojosa, H. Ji and J. Laterra, *J. Biol. Chem.*, 2014, **289**, 32742–32756.

44 K. C. Kondapalli, J. P. Llongueras, V. Capilla-González, H. Prasad, A. Hack, C. Smith, H. Guerrero-Cázares, A. Quiñones-Hinojosa and R. Rao, *Nat. Commun.*, 2015, **6**, 6289.

45 P. Schiapparelli, H. Guerrero-Cazares, R. Magaña-Maldonado, S. M. Hamilla, S. Ganaha, E. Goulin Lippi Fernandes, C.-H. Huang, H. Aranda-Espinoza, P. Devreotes and A. Quinones-Hinojosa, *EBioMedicine*, 2017, **21**, 94–103.

46 C. L. Smith, O. Kilic, P. Schiapparelli, H. Guerrero-Cazares, D.-H. Kim, N. I. Sedora-Roman, S. Gupta, T. O'Donnell, K. L. Chaichana, F. J. Rodriguez, S. Abbadi, J. S. Park, A. Quiñones-Hinojosa and A. Levchenko, *Cell Rep.*, 2016, **15**, 2616–2624.

47 S. Abbadi, J. J. Rodarte, A. Abutaleb, E. Lavell, C. L. Smith, W. Ruff, J. Schiller, A. Olivi, A. Levchenko, H. Guerrero-Cazares and A. Quinones-Hinojosa, *Mol. Cancer Res.*, 2014, **12**, 1547–1559.

48 J. C. Sunshine, D. Y. Peng and J. J. Green, *Mol. Pharm.*, 2012, **9**, 3375–3383.

49 F. Alexis, E. Pridgen, L. K. Molnar and O. C. Farokhzad, *Mol. Pharm.*, 2008, **5**, 505–515.

50 M. E. Katt, L. N. Mayo, S. E. Ellis, V. Mahairaki, J. D. Rothstein, L. Z. Cheng and P. C. Searson, *Fluids Barriers CNS*, 2019, DOI: 10.1186/s12987-019-0139-4.

51 J. D. Irvine, L. Takahashi, K. Lockhart, J. Cheong, J. W. Tolan, H. E. Selick and J. R. Grove, *J. Pharm. Sci.*, 1999, **88**, 28–33.

52 E. Garcia-Garcia, K. Andrieux, S. Gil and P. Couvreur, *Int. J. Pharm.*, 2005, **298**, 274–292.

53 K. E. Schlageter, P. Molnar, G. D. Lapin and D. R. Groothuis, *Microvasc. Res.*, 1999, **58**, 312–328.

54 P. Vajkoczy and M. D. Menger, *J. Neuro-Oncol.*, 2000, **50**, 99–108.